Broadband-tunable photonic bandgap and thermally-convertible laser with ultralow lasing threshold in a refilled chiral polymer template

Jia-De Lin,[a] Hsin-Yu Lin,[a] Guan-Jhong Wei,[a] Yu-Chou Chuang,[a] Lin-Jer Chen,[a] Ting-Shan Mo,[b] and Chia-Rong Lee[a]*

[a] *Department of Photonics, National Cheng Kung University, Tainan 701, Taiwan*

[b] *Department of Electro-Optical Engineering, Kun Shan University of Technology, Tainan 710, Taiwan*

Electronic Supplementary information

Improvement via thermal diffusion and rapid annealing process

The thermal diffusion and rapid annealing process can shorten the time for the formation of the pitch gradient in CLC and refine the gradient-pitched CLC. The defects in CLCs can be significantly reduced by rapid annealing process, as shown in Fig. S1.

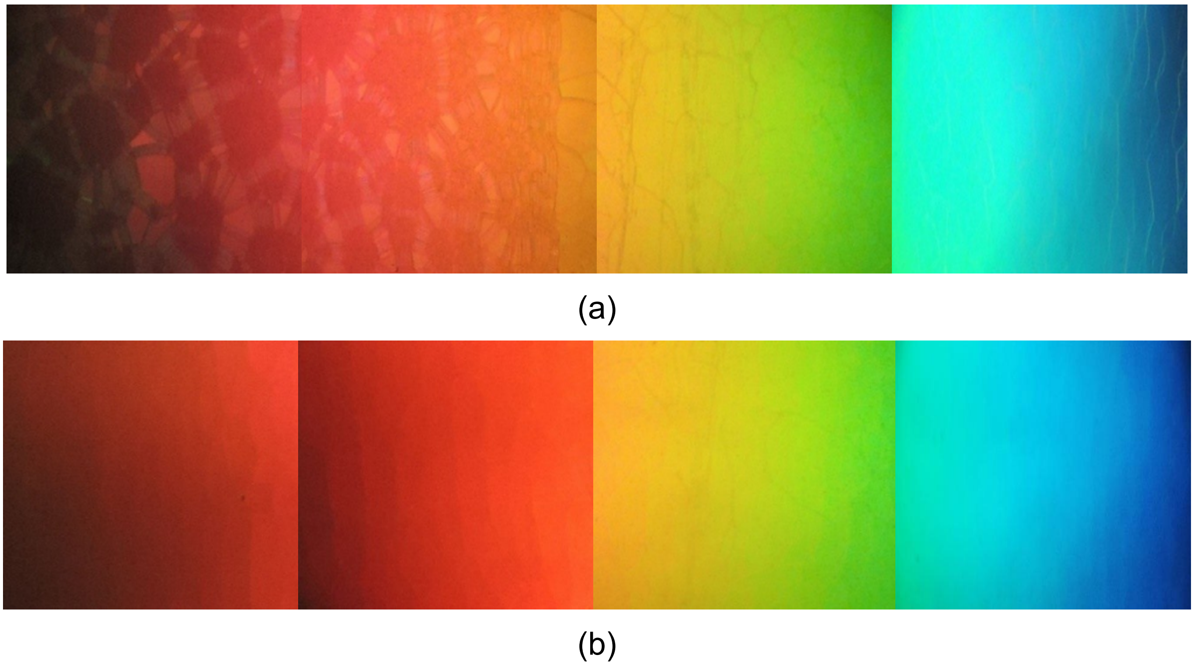

Figure S1. Reflective POM images of the gradient-pitched CLC (a) before and (b) after the rapid annealing process. The defects are significantly removed via the treatment of rapid annealing process.

Figures S2(a), S2(b), and S2(c) show the reflection spectra measured from $x = 0$ to $x = 15$ mm for the unrefined sample at before-curing, after-curing, and after-refilling stages, respectively. The corresponding reflection spectra for the refined sample at the three stages are also shown in Figures S2(d), S2(e), and S2(f), respectively, for comparison. Compared to the unrefined sample, the refined sample via thermal diffusion and rapid annealing process has the more uniform pitch gradient, as shown in Fig. S2.

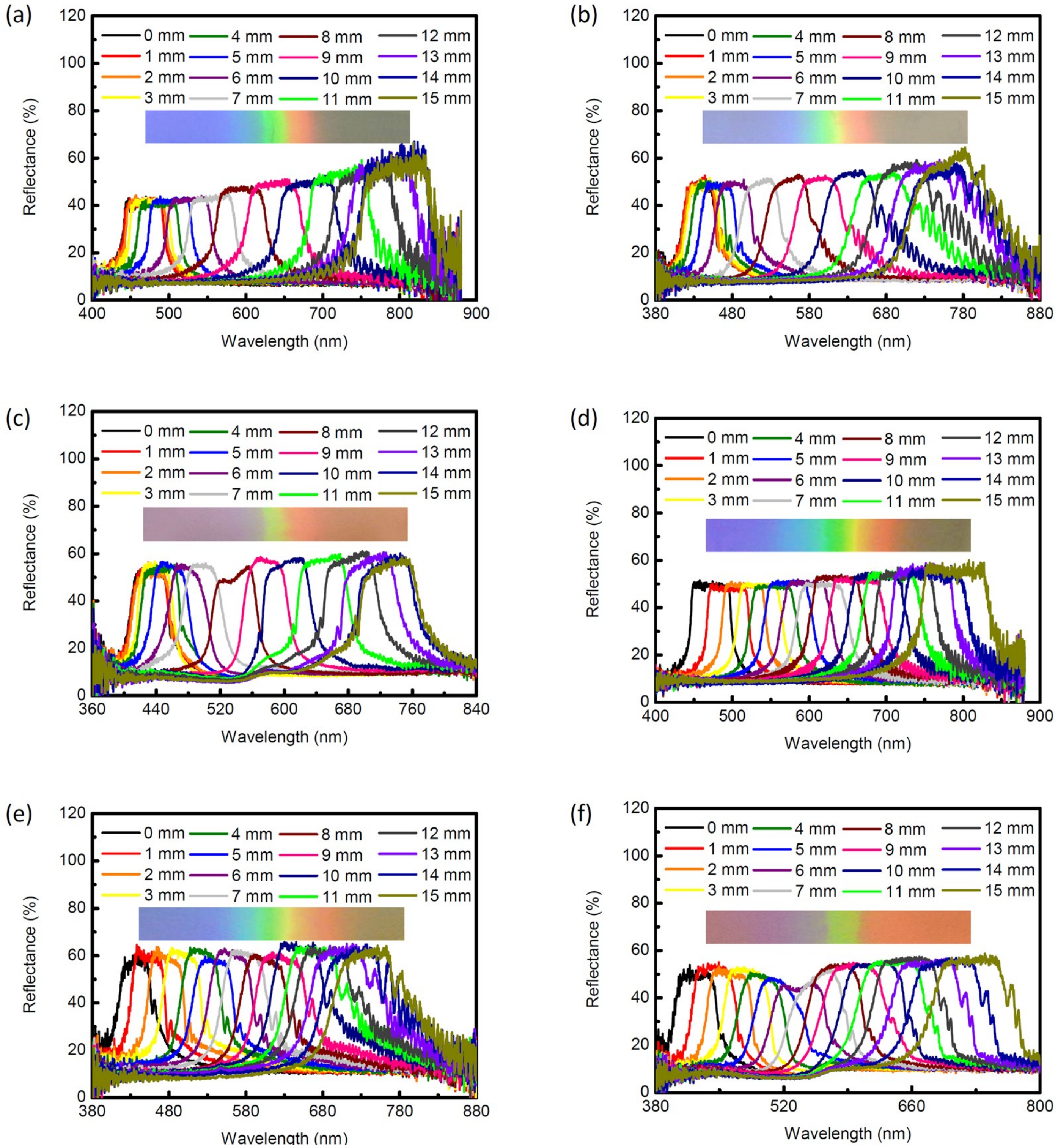

Figure S2. Reflection spectra and the corresponding reflective images inserted above the spectral curves at (a), (b), and (c) [(d), (e), and (f)] are before-curing, after-curing, and after-refilling stages based on the unrefined (refined) sample. The step of the measured position is 1.0 mm.

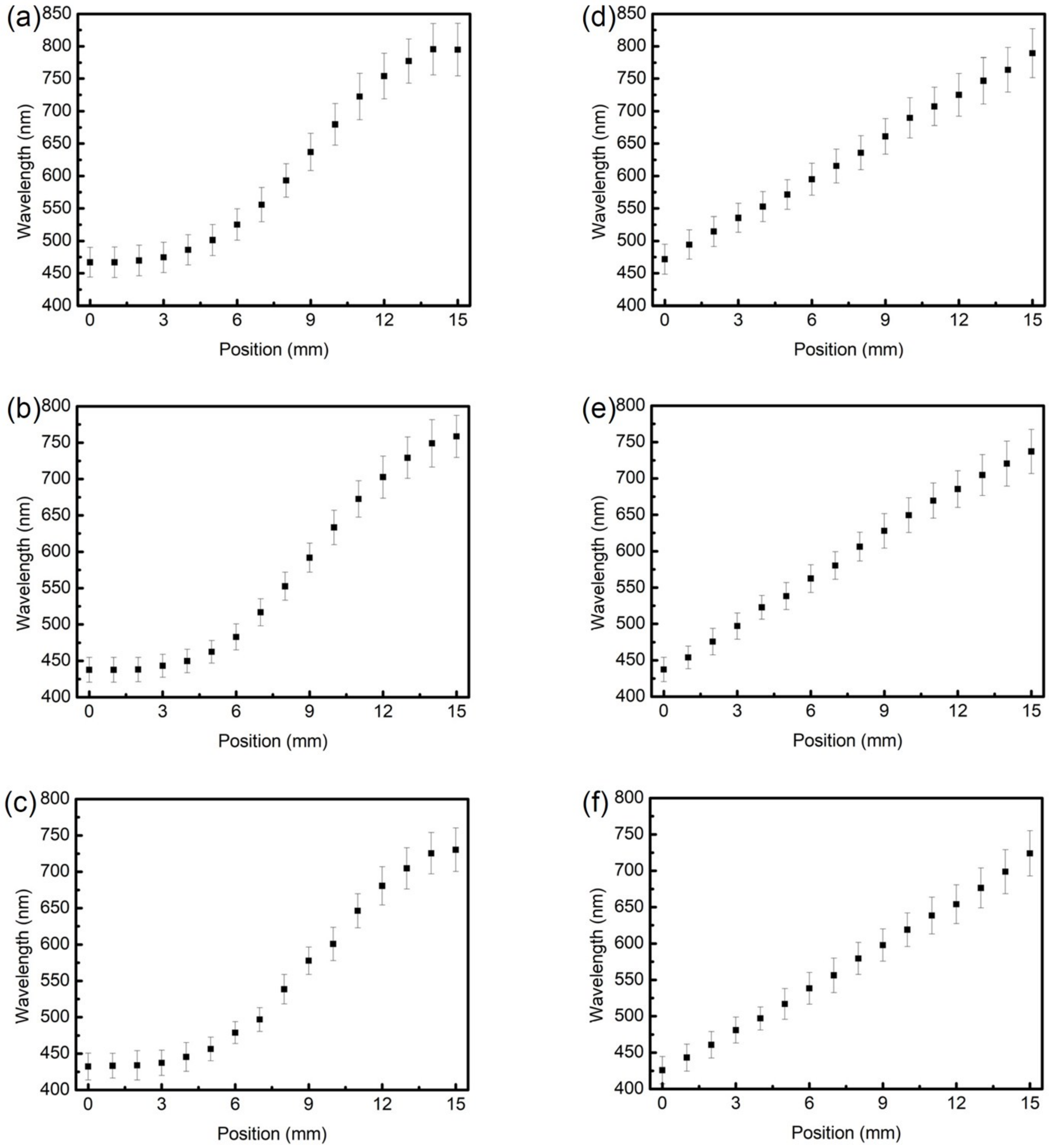

Figure S3. Relations between the central wavelength of the reflection λ_c and position presented at (a), (b), and (c) [(d), (e), and (f)] are before-curing, after-curing, and after-refilling stages based on the unrefined (refined) sample. The upper and bottom errors in each figure are representative for the long-wavelength edge (LWE) and short-wavelength edge (SWE) of the reflection band, respectively.

Schematic for the thermal convertibility between the multi-mode and single-mode lasing emissions

When the DDLC molecules are refilled into the nanopores of the template at the birefringent nematic phase, the director and thus the refractive index of the LCs slightly fluctuate at various sub-regions, resulting in the slight fluctuation in the effective refractive index of the refilled CLC template. The fluctuation in the effective refractive index of the refilled CLC template leads to the slight fluctuation in the PBG and its band-edges from one position to another in the same pumped region. Therefore, the multiple lasing peaks in the refilled CLC template sample at 22.4 °C can simultaneously appear at the slightly fluctuated band-edges of the PBG in each pumped region. In contrast, when the DDLC in the nanopores is heated to the isotropic state (44 °C), the refractive indices in these nanopores at various sub-regions of the same pumped region become identical inducing the almost identical PBG and thus the single-mode band-edge lasing emission at each pumped region.

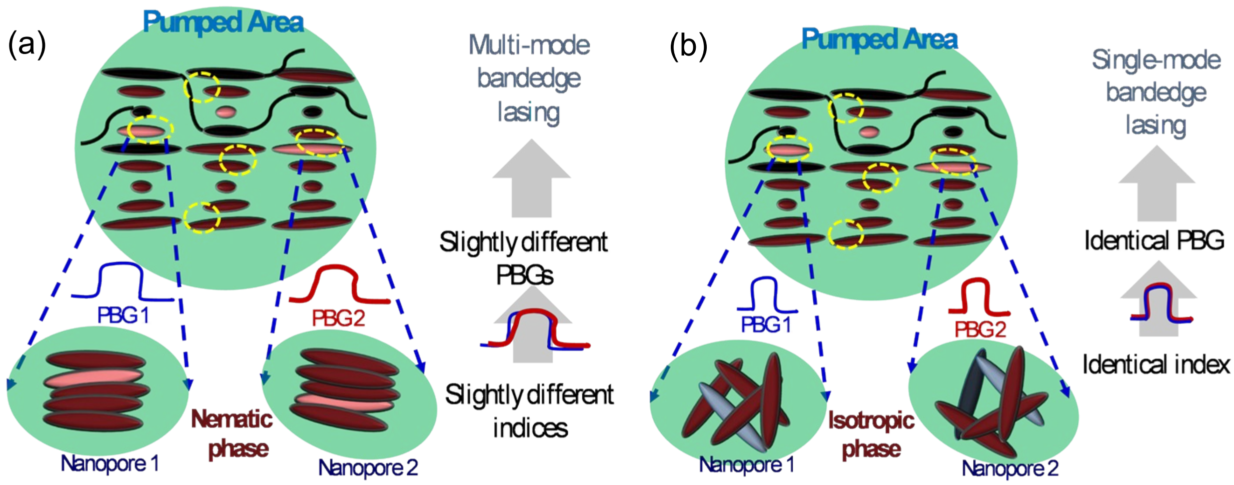

Figure S4. Schematics of the DDLC-refilled template sample when the refilled DDLC is at (a) nematic phase and (b) isotropic phase.

Energy thresholds of the refined DDNLC-refilled gradient-pitched template

The energy thresholds for the lasing emissions at various positions of the refined DDNLC-refilled gradient-pitched template can be determined by the variations of the peak intensity and the corresponding full-width at half-maximum (FWHM) with pumped energy at 22.4 °C and 44 °C, as presented in Figs. S5 and S6, respectively. When the pumped energy of the incident pulse is above the energy threshold, the peak intensity rises abruptly and the FWHM decreases dramatically, which is a typical fingerprint for lasing action. Figs. S5 and S6 show the measured results of the sample at pumped position x = 8.0, 9.0, 9.5, 10.0, 10.5, 11.2, 11.7, 12.2, 12.7, and 13.5 mm at 22.4 °C and 44 °C, respectively.

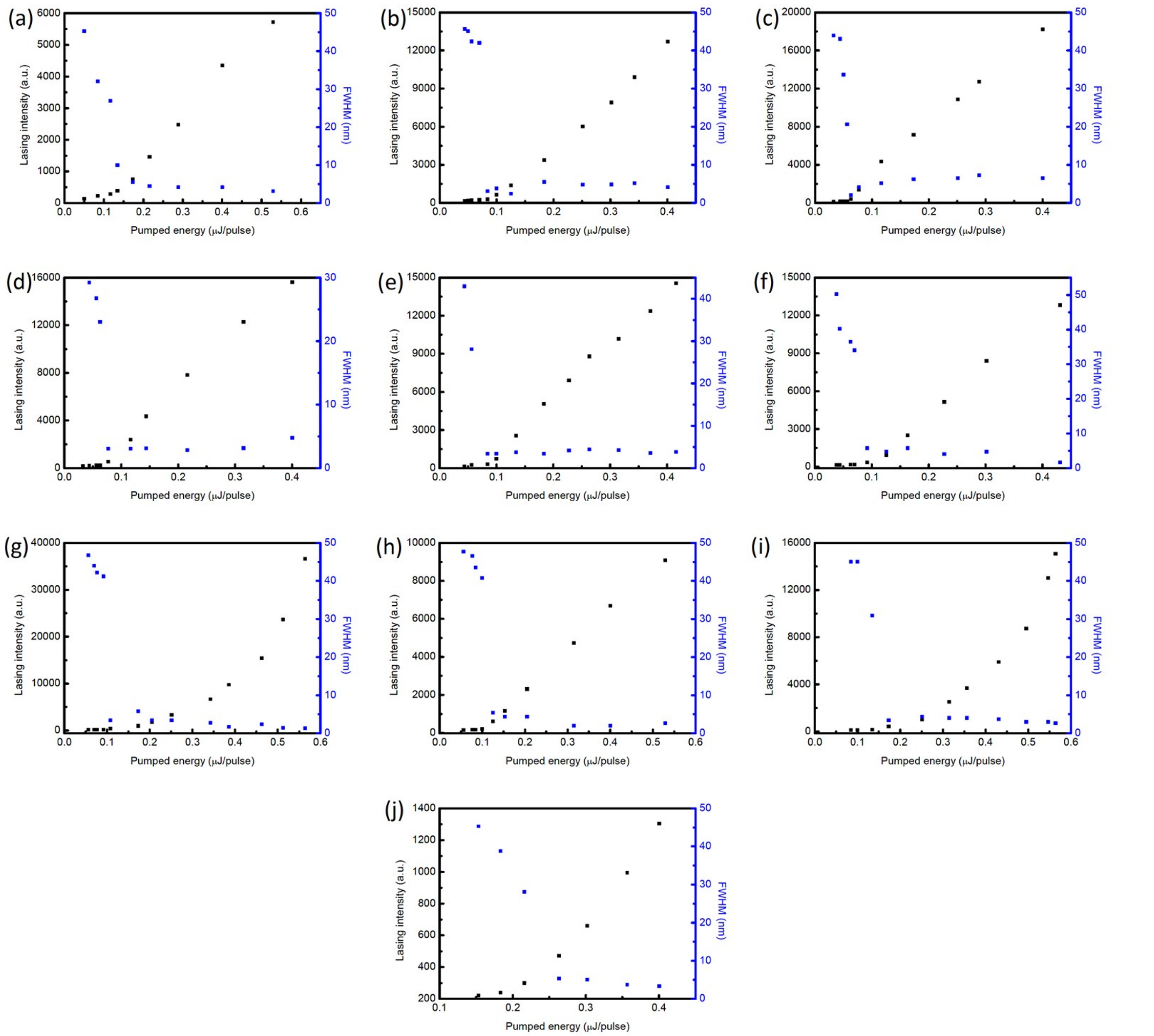

Figure S5. Variations of the intensity of the lasing peak and the corresponding FWHM of the multi-mode lasing emission for the refined DDNLC-refilled gradient-pitched template laser with pumped energy measured at positions of x = (a) 8.0, (b) 9.0, (c) 9.5, (d) 10.0, (e) 10.5, (f) 11.2, (g) 11.7, (h) 12.1, (i) 12.7, and (j) 13.5, respectively, at 22.4 °C.

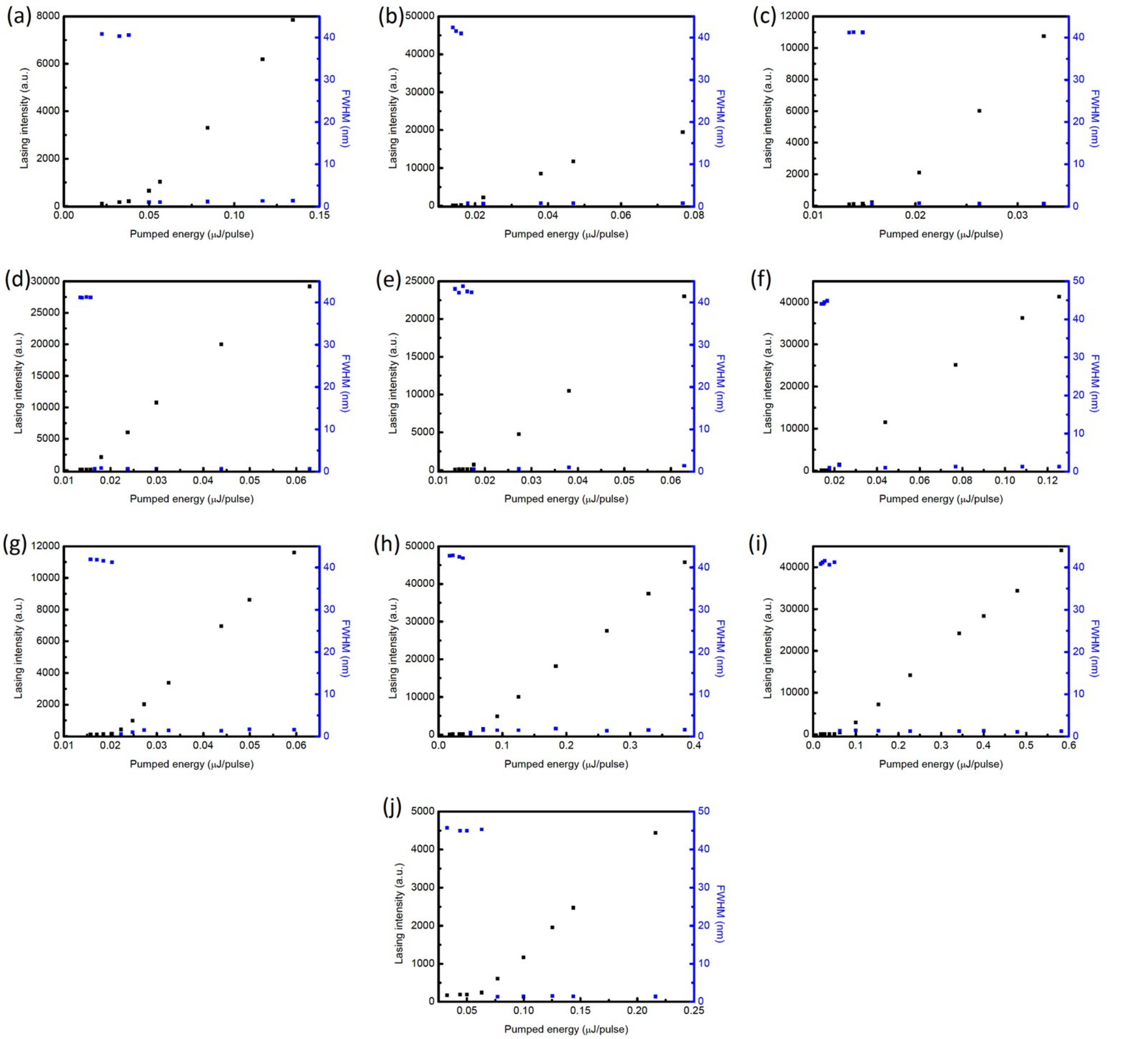

Figure S6. Variations of the intensity of the lasing peak and the corresponding FWHM of the single-mode lasing for the refined DDNLC-refilled gradient-pitched template laser with pumped energy measured at positions of x = (a) 8.0, (b) 9.0, (c) 9.5, (d) 10.0, (e) 10.5, (f) 11.2, (g) 11.7, (h) 12.1, (i) 12.7, and (j) 13.5, respectively, at 44.0 °C.

Lasing characteristics of the unrefined DDNLC-refilled gradient-pitched template

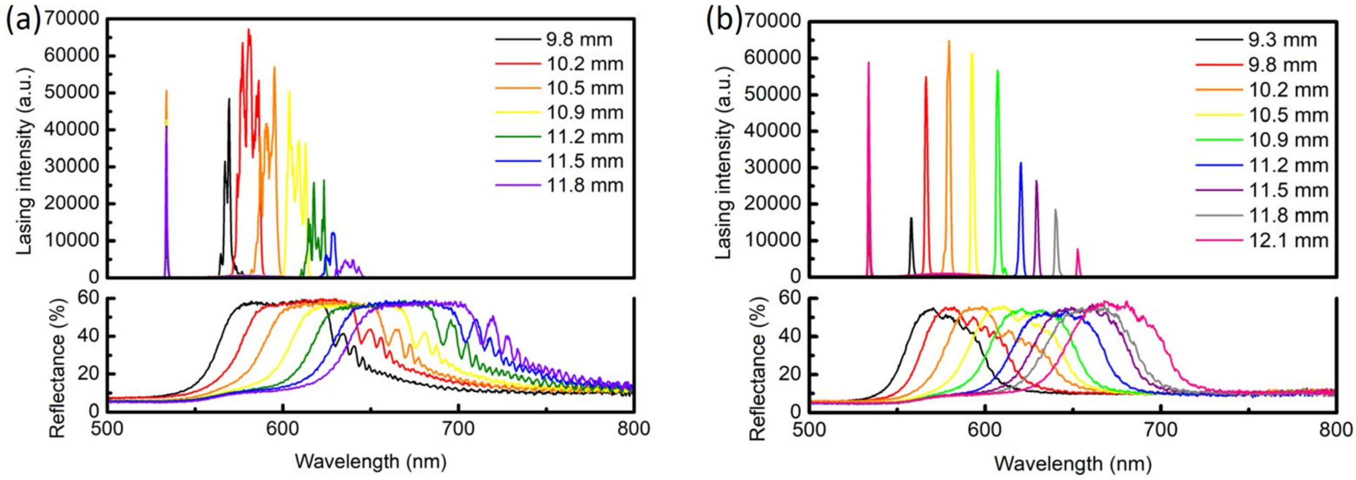

Figure S7. Lasing emission spectra attached with corresponding reflection spectra, presented below the lasing spectral curves, for the unrefined DDLC-refilled gradient-pitched template laser (a) at pumped positions of x = 9.8 mm to x = 11.8 mm and at T = 22.4 °C and E = 0.97 μJ/pulse and (b) at pumped positions of x = 9.3 mm to x = 12.1 mm and at T = 44 °C and E = 0.48 μJ/pulse.

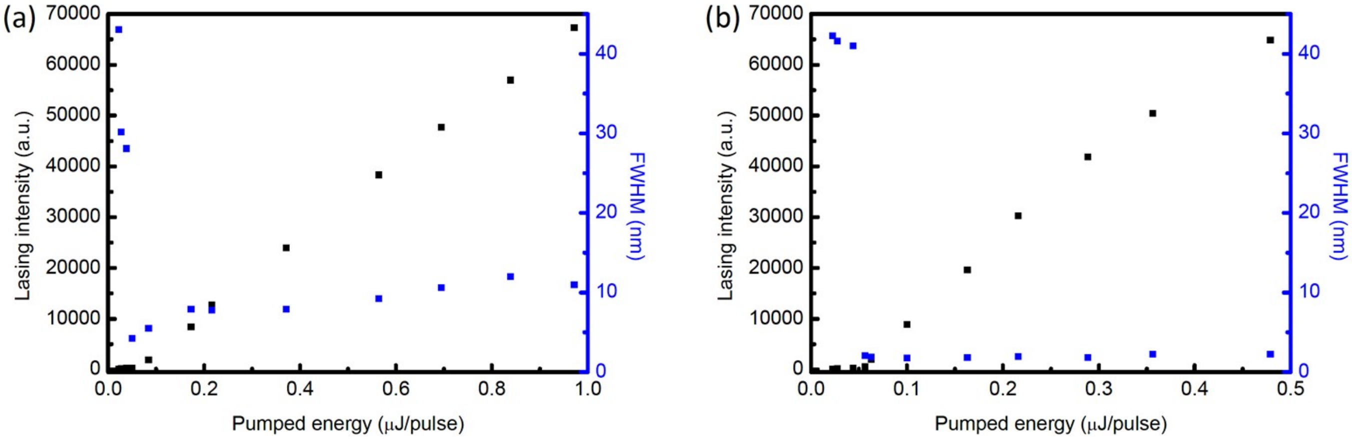

Figure S8. Variations of peak intensity of the fluorescence output and the corresponding FWHM with pumped energy for the strongest (a) multi-mode and (b) single-mode band-edge lasing emissions measured at x = 10.2 mm of the unrefined DDLC-refilled gradient-pitched template laser.